Journal of Power Sources 194 (2009) 704–711

Contents lists available at ScienceDirect

Journal of Power Sources

journal homepage: www.elsevier.com/locate/jpowsour

Structural, thermal and electrochemical properties of layered perovskite $SmBaCo_2O_{5+d}$, a potential cathode material for intermediate-temperature solid oxide fuel cells

Jung Hyun Kim [a], Yongmin Kim [a], Paul A. Connor [b], John T.S. Irvine [b,*], Joongmyeon Bae [a,**], Wuzong Zhou [b]

[a] Department of Mechanical Engineering, Korea Advanced Institute of Science and Technology, 373-1 Guseong-Dong, Yuseong-Gu, Daejeon 305-701, Republic of Korea
[b] School of Chemistry, University of St. Andrews, St. Andrews, Fife KY16 9ST, United Kingdom

ARTICLE INFO

Article history:
Received 11 March 2009
Received in revised form 5 May 2009
Accepted 3 June 2009
Available online 18 June 2009

Keywords:
Layered perovskite
Solid oxide fuel cell
Cathode
Electrical conductivity
Area specific resistance

ABSTRACT

The synthesis, conductivity properties, area specific resistance (ASR) and thermal expansion behaviour of the layered perovskite $SmBaCo_2O_{5+d}$ (SBCO) are investigated for use as a cathode material for intermediate-temperature solid oxide fuel cells (IT-SOFCs). The SBCO is prepared and shows the expected orthorhombic pattern. The electrical conductivity of SBCO exhibits a metal–insulator transition at about 200 °C. The maximum conductivity is 570 S cm^{-1} at 200 °C and its value is higher than 170 S cm^{-1} over the whole temperature range investigated. Under variable oxygen partial pressure SBCO is found to be a p-type conductor. The ASR of a composite cathode (50 wt% SBCO and 50 wt% $Ce_{0.9}Gd_{0.1}O_{2-d}$, SBCO:50) on a $Ce_{0.9}Gd_{0.1}O_{2-d}$ (CGO91) electrolyte is 0.05 Ω cm^2 at 700 °C. An abrupt increase in thermal expansion is observed in the vicinity of 320 °C and is ascribed to the generation of oxygen vacancies. The coefficients of thermal expansion (CTE) of SBCO is 19.7 and 20.0 × 10^{-6} K^{-1} at 600 and 700 °C, respectively. By contrast, CTE values for SBCO:50 are 12.3, 12.5 and 12.7 × 10^{-6} K^{-1} at 500, 600 and 700 °C, that is, very similar to the value of the CGO91 electrolyte.

1. Introduction

Most research on intermediate-temperature operating solid oxide fuel cells (IT-SOFCs) is devoted to cathode materials as the cathode overpotential has typically been the major source of voltage loss in IT-SOFC operation [1–3]. Cathode materials for IT-SOFCs have focused on mixed ionic and electronic conductors (MIECs) such as $LaCoO_3$, $(La,Sr)CoO_3$, $BaCoO_3$ and $(Ba,Sr)CoO_3$ doped with transition ions that show excellent catalytic activity [4–7].

Recently, several research groups have reported structural and physical properties of layered perovskites based on $LnBaCo_2O_{5+d}$ (Ln: lanthanide) [8,9], from investigations of the colossal magnetoresistance (CMR) phenomenon [10–13] as well as in a solid oxide fuel cell (SOFC) [14,15]. These layered perovskites have orthorhombic symmetry that displays two types of Co–O environment, $Co–O_5$ square pyramids and $Co–O_6$ octahedra, which alternate along the *b*-axis (0 0 1) [16,17]. The structure of $LnBaCo_2O_{5+d}$ has layers of [Ba–O], [Co–O] and [Ln–O] aligned along the *C*-axis (0 0 1 direction) with oxygen vacancies as clusters in the [Ln–O] layer [18]. For example, all oxygen vacancies are located at the rare earth plane $[Gd–O]_x$ for $d < 1$ in $GdBaCo_2O_{5+d}$ [19]. In this structure, the Ba cations do not show a random distribution in the A site of perovskite but tend to order in altering layers [19].

The structure of $LnBaCo_2O_{5+d}$ (Ln:lanthanide) can have a tetragonal or orthorhombic unit cell depending on the size of the lanthanide [9,20–23]. For example, the structure with the smaller rare earth ions such as Tb, Dy and Ho or the larger rare earth ions such as Pr and Nd in $LnBaCo_2O_{5+d}$ are tetragonal. On the other hand, the intermediate-sized rare earth ions for Sm, Eu and Gd in $LnBaCo_2O_{5+d}$ are orthorhombic [9,20–23].

Various physical properties of layered perovskite oxides depend on the oxygen content (*d*). For example, the charge state of Co is 3.5+ when *d* is 1, whereas in case of $d = 0.5$, the Co charge state is 3+ and metal–insulator transition (MIT) behaviour can be observed with various lanthanide elements [20,24–29]. As a result, orbital ordering phenomena and spin-state transitions of Co in octahedral places have been observed in this system [25,30]. Finally, for $d = 0$, Co has an overall 2.5+ charge state with a charge ordering between Co^{3+} and Co^{2+} [20,25–29].

As well as high electronic conductivity, recent results show high oxygen transport properties, excellent oxygen surface exchange coefficients and superior oxide ionic diffusivity for layered perovskite oxides [31,32] and thus make them good candidates for

* Corresponding author. Tel.: +44 1334 463817; fax: +44 1334 463808.
** Corresponding author. Tel.: +82 42 350 3045; fax: +82 42 350 8207.
E-mail addresses: jtsi@st-andrews.ac.uk (J.T.S. Irvine), jmbae@kaist.ac.kr (J. Bae).

0378-7753/$ – see front matter © 2009 Elsevier B.V. All rights reserved.
doi:10.1016/j.jpowsour.2009.06.024

Table 1
Abbreviations of specimens.

Chemical composition	Abbreviations
$Ce_{0.9}Gd_{0.1}O_{2-d}$	CGO91
$SmBaCo_2O_{5+d}$	SBCO
$SmBaCo_2O_{5+d}$ (90 wt%) and $Ce_{0.9}Gd_{0.1}O_{2-d}$ (10 wt%)	SBCO:10
$SmBaCo_2O_{5+d}$ (80 wt%) and $Ce_{0.9}Gd_{0.1}O_{2-d}$ (20 wt%)	SBCO:20
$SmBaCo_2O_{5+d}$ (70 wt%) and $Ce_{0.9}Gd_{0.1}O_{2-d}$ (30 wt%)	SBCO:30
$SmBaCo_2O_{5+d}$ (60 wt%) and $Ce_{0.9}Gd_{0.1}O_{2-d}$ (40 wt%)	SBCO:40
$SmBaCo_2O_{5+d}$ (50 wt%) and $Ce_{0.9}Gd_{0.1}O_{2-d}$ (50 wt%)	SBCO:50

IT-SOFC cathodes. To date however, there appears to be no published study on the application of a composite cathode based on layered perovskite materials.

The purpose of this work is to investigate the structural, electrochemical and thermal properties of $SmBaCo_2O_{5+d}$ (SBCO) for its application as a cathode material for IT-SOFC. The electrochemical and thermal expansion properties of a SBCO/$Ce_{0.9}Gd_{0.1}O_{2-d}$ (CGO91) composite cathode are measured and discussed in order to determine its suitability for IT-SOFC materials.

2. Experimental

2.1. Sample preparation and X-ray diffraction analysis

The SBCO was made from samarium oxide (Sm_2O_3), barium carbonate ($BaCO_3$) and cobalt oxide (Co_3O_4). Weighed powders were mixed, ground in a mortar and pestle, and then placed in a muffle furnace at 1000 °C for 8 h as a first calcination step, in order to decompose all the carbonate. The resulting powder was milled (in a roller ball mill) for 24 h with acetone, then the heat treatment was repeated at 1100 °C for 36 h. The notations for the samples are summarized in Table 1. X-ray diffraction patterns of the prepared samples were recorded on a Philips diffractormeter using Cu Kα radiation. The collected data were matched with reference data for the identification of crystal structures.

2.2. Thermal expansion behaviour and thermal analysis

Pellets for the investigation of thermal expansion behaviour were prepared by pressing a rectangular-shaped bar type (5 mm × 5 mm × 18 mm) and sintering at 1100 °C for 12 h in air. The coefficient of thermal expansion (CTE) of the samples was measured with a NETZSCH DIL 402C dillatometer from room temperature to 1000 °C at a heating rate of 5 °C min^{-1}. For thermal analysis, thermogravimetric analysis (TGA)–differential scanning calorimeter (DSC) experiments were performed with a thermal analyzer (SETRAM Labsys). About 100 mg powder sample was heated to 900 °C at heating rate of 5 °C min^{-1} in air.

2.3. Electrochemical characterization and conductivity properties

Pellets for electrical conductivity were pressed and then were sintered at 1100 °C for 12 h in air. A rectangular-shaped bar (3 mm × 3 mm × 8.5 mm) was cut from the sintered pellet. The conductivities were measured by using a 4 terminal d.c. method and a custom jig with a Keithley 2400 Source Meter over a temperature range of 50–900 °C with steps of 50 °C at a rate of 5 °C min^{-1}. The expression used for the temperature dependence of the electrical conductivity is

$$\sigma = \left(\frac{A}{T}\right) \exp\left(-\frac{E_a}{KT}\right) \quad (1)$$

where A is the pre-exponential factor which includes the carrier concentration term, T is the absolute temperature, k is the Boltzmann's constant ; E_a is the hopping activation energy [1,33,34]. The oxygen partial pressure was controlled by using air and argon gas and measured with airconia oxygen sensor.

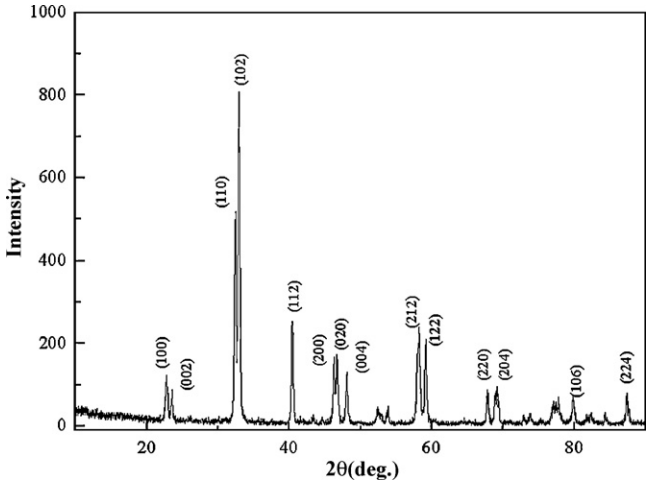

Fig. 1. X-ray diffraction pattern of $SmBaCo_2O_{5+d}$ (SBCO) calcined at 1100 °C for 36 h.

Impedance spectroscopy was used to investigate the current–voltage behaviour of symmetrical cells. The electrolytes were made from 10 mol% gadolinia-doped ceria ($Ce_{0.9}Gd_{0.1}O_{2-d}$, CGO91, Praxair Specialty Ceramics) by pressing the powder into 22 mm diameter pellets at 2×10^3 kg m^{-2} and sintering at 1400 °C for 4 h. The final geometry of the sintered electrolyte pellets was approximately 21 mm in diameter and 2 mm in thickness.

Inks of both single-phase cathodes, and composite cathodes with CGO91, were made by mixing the powders with the appropriate solvent and binder system. The electrodes were then applied to the electrolytes using screen printing to form symmetrical half-cells. These were sintered for 1 h at 900, 1000, 1100 or 1200 °C in order to determine the optimum sintering temperature to form a porous electrode structure well-bonded to the electrolyte. The final surface area of the symmetric cell was about 1.09 cm^2.

The area specific resistances (ASRs) of single and composite cathodes in $SmBaCo_2O_{5+d}$ (SBCO) were measured via a.c. impedance with a Solatron 1260 frequency analyzer over a frequency range of 0.01 Hz to 1 MHz with an amplitude of 50 mV. The samples were measured in stagnant air from 500 to 850 °C with 50 °C steps. The cathode overpotential polarization was determined from the difference between the low and high frequency intercepts on the real axis of the impedance curves, divided by 2.

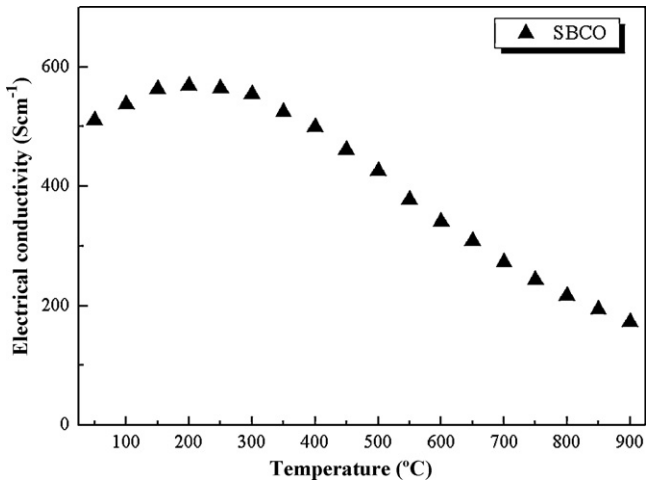

Fig. 2. Electrical conductivity of SBCO as function of temperature.

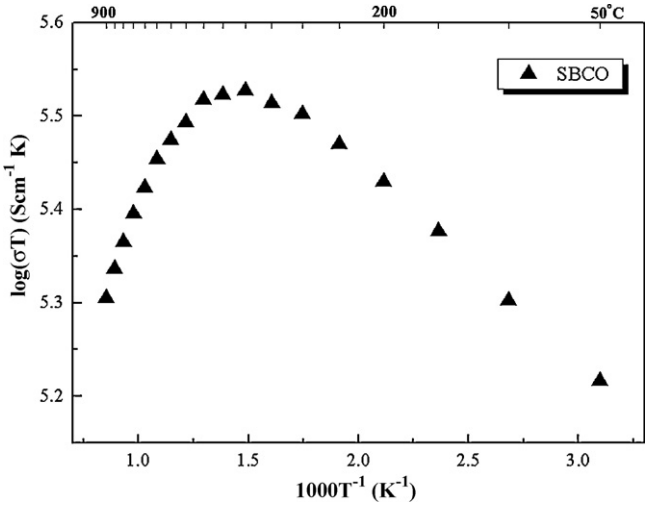

Fig. 3. Electrical conductivity plot of SBCO with $\log(\sigma T)$ versus $1000\,T^{-1}$ (K^{-1}).

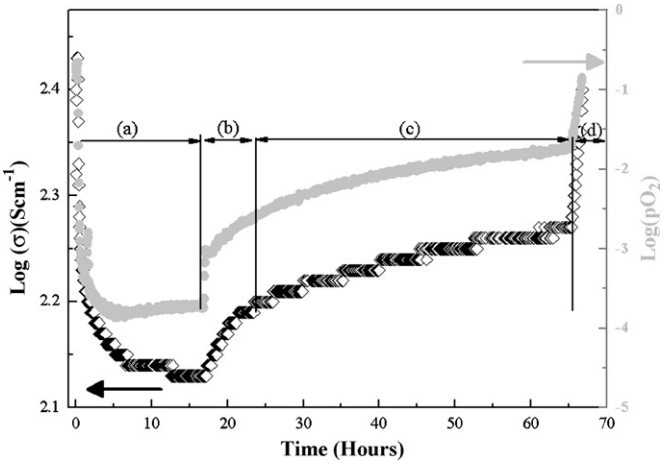

Fig. 4. Electrical conductivity behaviour of SBCO at 900 °C. Results show different electrical conductivities of SBCO with respect to reduction and oxidation process controlled by supplying Ar gas. Black open scatter is electrical conductivity of SBCO and gray close scatter of zirconia oxygen sensor.

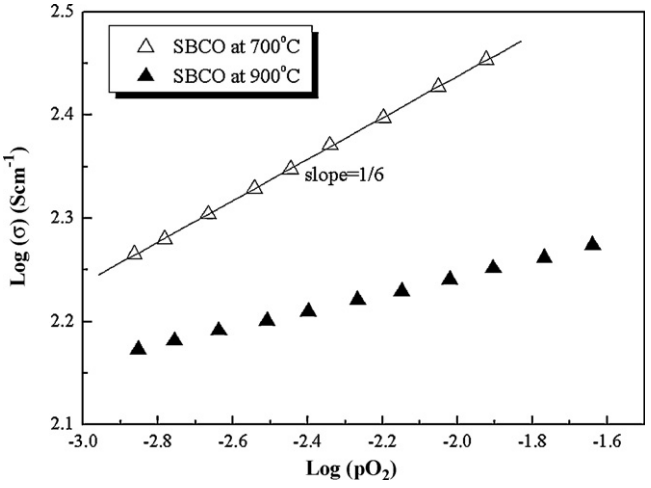

Fig. 5. Variation of electrical conductivity of SBCO with oxygen partial pressure at 700 and 900 °C.

3. Results and discussion

The X-ray diffraction (XRD) pattern of $SmBaCo_2O_{5+d}$ (SBCO) after the second calcination at 1100 °C for 36 h is presented in Fig. 1 The XRD pattern of SBCO is represented at a single-phase layered per-

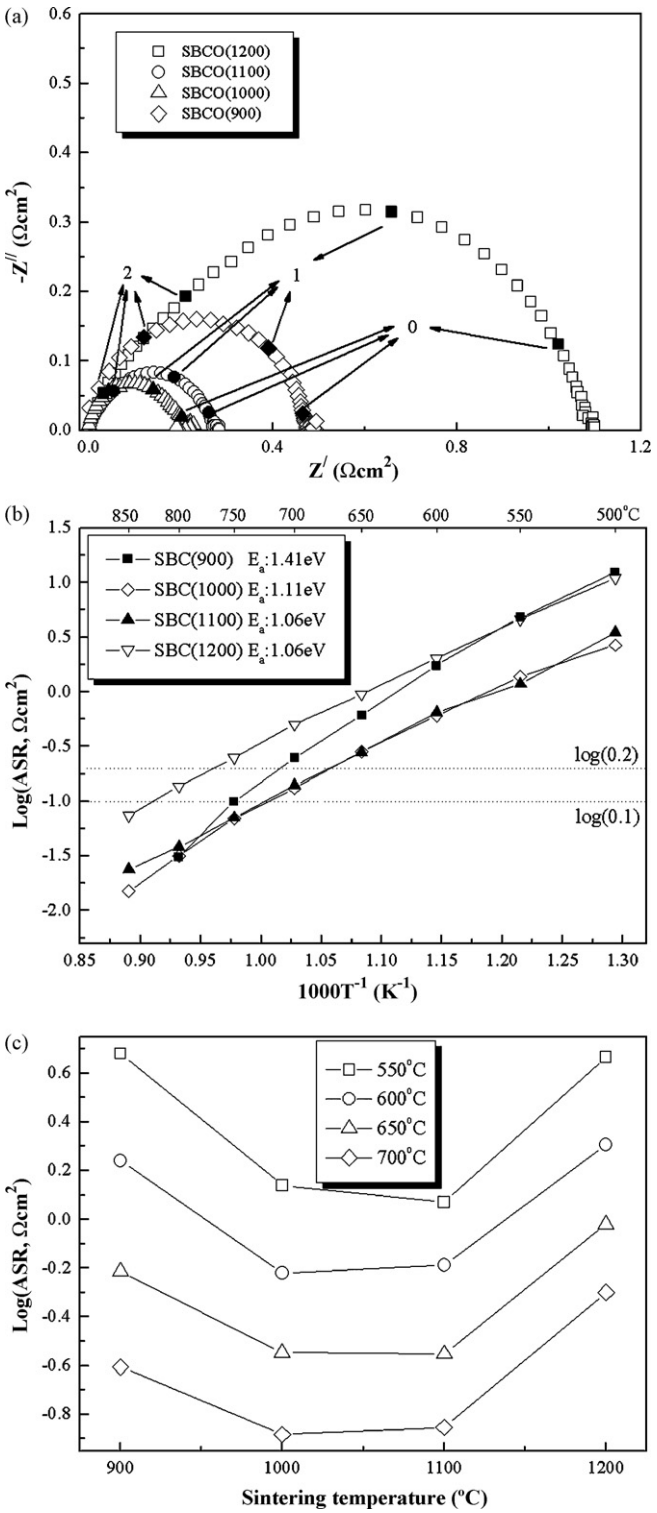

Fig. 6. (a) Comparison of impedance results on various samples sintered at 900, 1000, 1100 and 1200 °C. (b) Area specific resistance (ASR) results shown as Arrhenius plot of SBCO. Number in bracket indicates sintering temperature from 900 to 1200 °C for 1 h. Error range of the estimated activation calculation is ±0.01 eV and (c) ASR values from 550 to 700 °C on CGO91 electrolyte.

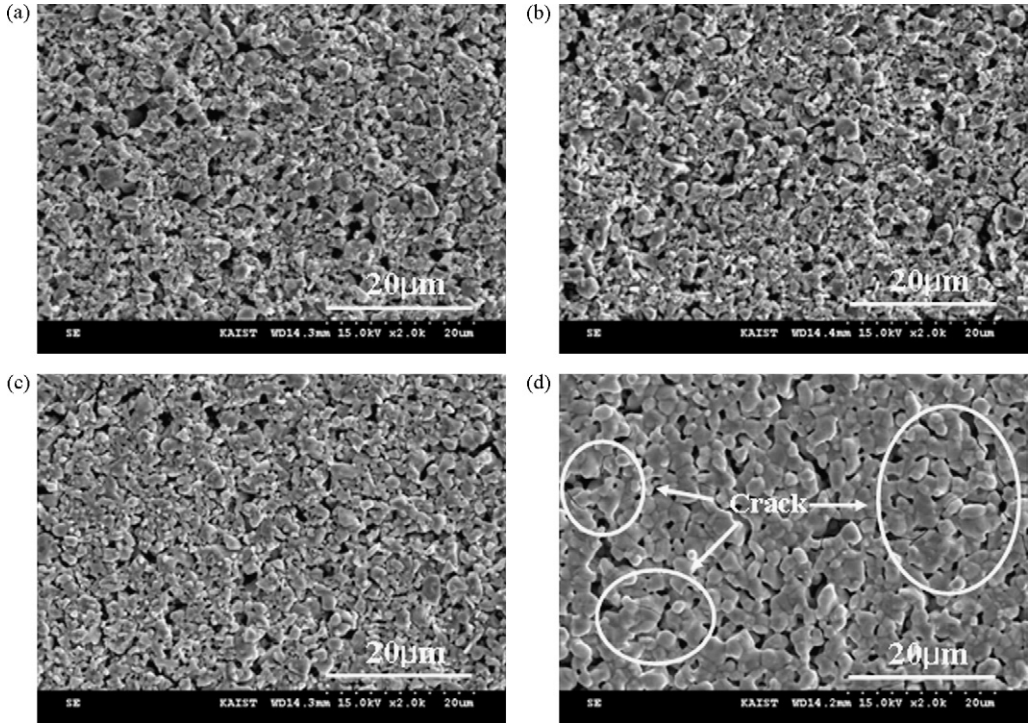

Fig. 7. Scanning electron microscopic images of electrode surfaces of SBCO with sintered at (a) 900 °C, (b) 1000 °C, (c) 1100 °C and (d) 1200 °C.

ovskite without any impurity phase; the indexed primary peaks of SBCO are summarized in Fig. 1 [14]. Early work has shown [9] that shows the substitution of the Ba cation to form a layered perovskite of $YBaCo_2O_{5+d}$ gives a tetragonal unit cell with $a = 3.887$ Å and $c = 7.530$ Å. The structure is orthorhombic in nature and is also consistent with $GdBaCo_2O_{5+d}$ (GBCO), as reported by Tarancón et al. [35]. According to the study by Zhang et al. [36], the orthorhombic structure of SBCO was observed as $a = 3.866$ Å, $b = 3.885$ Å and $c = 7.569$ Å with a *Pmmm* space group.

The electrical conductivity of SBCO, Fig. 2, initially increases, reaches a maximum value (570 S cm^{-1} around 200–250 °C), and then decreases with increasing temperature, showing a metal–insulator transition (MIT). The lowest electrical conductivity of SBCO at 900 °C is still above 170 S cm^{-1} and therefore the material

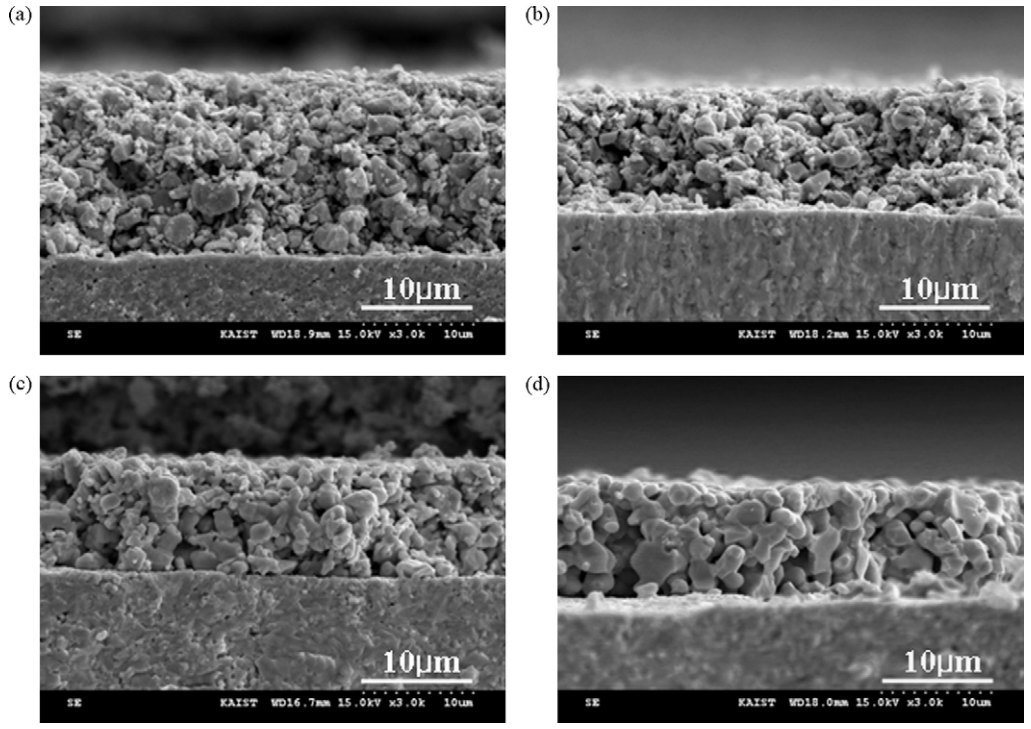

Fig. 8. Scanning electron microscopic images of cross-section of samples of SBCO with sintered at (a) 900 °C, (b) 1000 °C, (c) 1100 °C and (d) 1200 °C.

is adequate for application as a cathode in a IT-SOFC. The apparent metallic conductivity behaviour of SBCO above 250 °C may relate to an energy band overlap between Co-3d and O-2p [37] and the presence of Co^{4+} ions from thermally generated charge disproportion of Co^{3+}, although it may also relate to oxygen loss on heating, as this is observed to occur above 300 °C. The data are also presented as a $\log(\sigma T)$ versus $1000\,T^{-1}$ (K^{-1}) plot in Fig. 3, and are consistent with small polaron hopping at lower temperatures; the activation energy of SBCO from room temperature towards 300 °C is about 0.017 eV.

Fig. 4 shows the conductivity behaviour versus time on changing the oxygen partial pressure at 900 °C. The oxygen partial pressure is varied by introducing argon gas and then allowing air to leak back into the apparatus. The black open points indicate the electrical conductivity of SBCO, where as the gray closed points show oxygen partial pressure measured via a zirconia oxygen sensor. The variation in electrical conductivity with respect to oxygen partial pressure can be described by four regions, namely, a, b, c and d in Fig. 4. Region (a) presents a decrease in the electrical conductivity of SBCO after the introduction of flowing Ar, (b) is the change in response after switching off the Ar flow, region (c) is the slow oxidation process during air leakage and, finally, the abrupt increase of electrical conductivity in region (d) coincides with the rapid addition of air. From this and a similar experiment at 700 °C, it can be seen that SBCO shows p-type electrical conductivity properties, and that the conductivity decreases with temperature, Fig. 5. In the 700 °C regime, the slope of $\log(\sigma)$ versus $\log(p(O_2))$ is calculated as 1/6. In the oxidation region, therefore, the conductivity is theoretically proportional to $p(O_2)^{1/6}$. On the other hand, the slope at 900 °C is smaller than that of conductivity at 700 °C due to the high temperature effect and mixed conductivity effect caused by hole conduction and oxygen vacancies.

Impedance spectra of SBCO with respect to various sintering temperatures are shown in Fig. 6(a); the number in bracket indicates the sintering temperature. The results presented in Fig. 6(a) have the ohmic resistance removed in order to compare polarization of the cathode. The cathode sintered at 1000 °C shows the lowest cathodic polarization (Rp) in this experiment. The effects of sintering temperature on ASR of a SBCO cathode on a $Ce_{0.9}Gd_{0.1}O_{2-d}$ (CGO91) electrolyte are measured at various temperatures in Fig. 6(b); the number in bracket indicates the specific sintering temperature. Sintering temperatures of 1000 and 1100 °C result in the lowest ASR values of 0.13 and 0.14 $\Omega\,cm^2$ at 700 °C as seen in Fig. 6(c). The observed activation energies of SBCO are 1.41, 1.11, 1.06 and 1.06 eV (±0.01 eV) for the samples sintered from 900 to 1200 °C as seen in Fig. 6(b). Comparing the activation energies of the samples, the value for 900 °C is much higher than those sintered at the higher temperatures and this feature can be related to changes in the microstructure. The microstructures of samples with various sintering temperatures are given in Figs. 7 and 8. The sample sintered at 1200 °C shows both increased density and reduced relative porosity in Figs. 7(d) and 8(d), compared with the others. This correlates with the higher Rp observed for the 1200 °C sintered samples. Additionally, cracks in the 1200 °C sintered sample are observed after the sintering process and can result in isolated electronic and ionic current paths. In summary, the densification of the SBCO cathode and the evidence of cracking in the 1200 °C sintered sample seems to increase Rp. The 900 °C sintered sample shows relatively poor adhesion between the cathode and the CGO91 electrolyte side (Figs. 7(a) and 8(a)) because it is easily peeled off when subjected to an adhesion test. This poor contact increases both the series and the polarization resistance. The higher activation energy (1.41 eV) for the 900 °C sintered sample observed in Fig. 6(b) and the microstructure seen in Figs. 7(a) and 8(a) suggests insufficient sintering. According to the results from Figs. 6–8, the optimum sintering temperature of a symmetrical half-cell with a SBCO cathode is 1000 °C as it simultaneously provides the best balance between the conflicting electrode requirements, maintains a porous, high-surface area structure, and provides a strong, well-sintered and adherent layer. Consequently, the following experiments are based on a sintering temperature of 1000 °C for symmetrical half-cells.

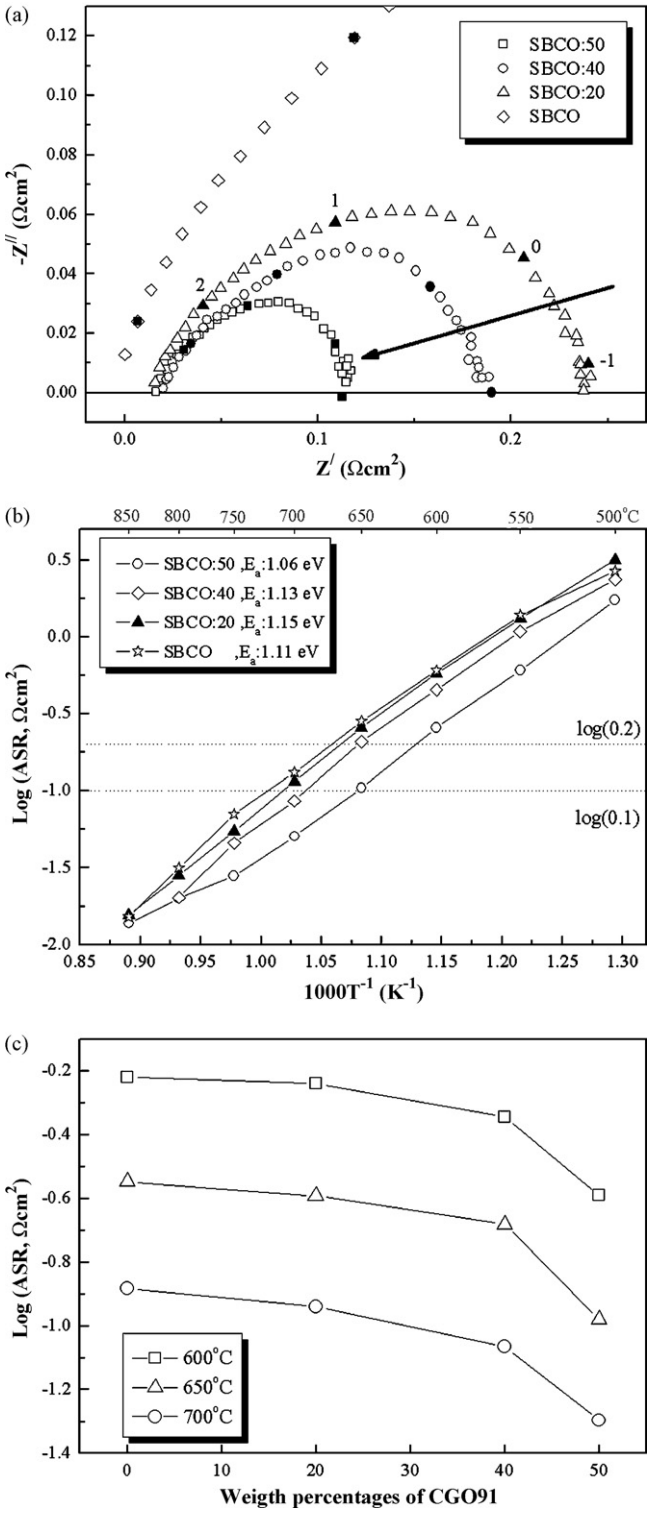

Fig. 9. (a) Comparison of impedance spectra of composite cathode-based SBCO and CGO91 measured at 700 °C on CGO91. (b) ASR results of composite cathode materials on CGO91 and (c) ASR results as function of weight percentages of CGO91 as composite cathode from 600 to 700 °C on CGO91.

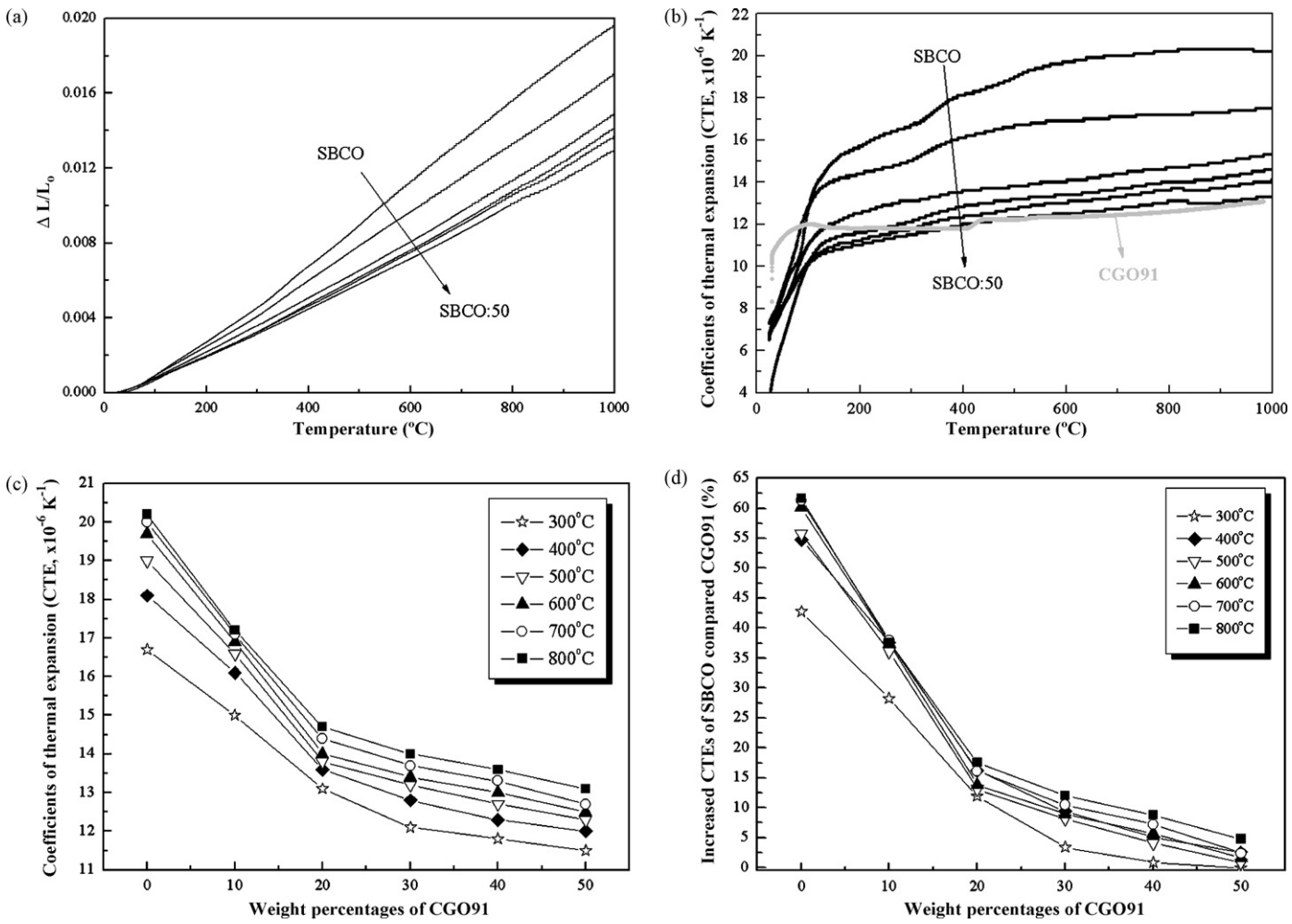

Fig. 10. Coefficients of thermal expansion (CTEs) of SBCO in air. (a) Thermal expansion curve with increasing temperature, (b) coefficient of thermal expansion (CTE) and CGO91 as function of temperature, (c) CTE results with weight percentage of CGO91 with SBCO at 300, 400, 500, 600, 700 and 800 °C; (d) relative CTE values compared with CGO91. The values in (d) are expressed as percentages.

Impedance spectra of SBCO:50 (mixture of 50 wt% of SBCO and 50 wt% of CGO91) are shown in Fig. 9(a). The ASRs of SBCO:50 at 600 and 700 °C are 0.25 and 0.05 Ω cm^2, respectively. The influence of changes in the CGO91 content on Rp at 700 °C is shown in Fig. 9(a). The ASR decreases when the content of CGO91 is increased. This is most likely due to an extended electrochemical triple-phase boundary (TPB) and enhanced oxygen diffusion as a result of the addition of the ionic conducting electrolyte material. The ASRs of composite cathodes are presented in Fig. 9(b). The total ASR values generally decreases with CGO91 content and the activation energies are approximately 1.11, 1.15, 1.13 and 1.06 eV (±0.01 eV) for SBCO, SBCO:20, SBCO:40 and SBCO:50, although there are some small deviations from linearity. The ASR values depend strongly upon the CGO91 weight percentage, as shown in Fig. 9(c). The lowest observed ASR value at 700 °C is 0.05 Ω cm^2 for SBCO:50 and is below the target ASR value recommended by Steele and Heinzel [38] for cathode materials for IT-SOFCs.

Thermal expansion data for SBCO, the composite cathodes and pure CGO91 are given in Fig. 10. The thermal expansion behaviour of SBCO shows slope changes at about 100 and 320 °C (Fig. 10(a)). The degree of expansion decreases with an increasing amount of CGO91 in the composite. The slope change, $\Delta L/L_o$, in the vicinity of 320 °C can be related to the generation of oxygen vacancies as a result of oxygen loss in SBCO due to loss of lattice oxygen; this is similar to the behaviour of (Ba,Sr)(Co,Fe)O_{3-d} [33].

Similar coefficients of thermal expansion (CTEs) between the cathode and the electrolyte are required to avoid significant thermal stresses which can cause delamination and cracks [39]. The CTE of pure SBCO is much higher than that of CGO91, but the data in Fig. 10(b) shows that the CTE of the composite is reduced with increasing CGO91 content, with the lowest value observed for SBSCO:50. Significantly, the average CTEs of SBCO:50 and CGO91 are similar from 350 to 1000 °C. The CTEs of various electrolyte and cathode materials for SOFC application between room temperature (RT) and 1000 °C are summarized in Table 2 [1,33,34,40–43]. From these data, it can be seen that Co-substituted cathode materials, such as $Sm_{0.5}Sr_{0.5}CoO_{3-d}$ [34,39] and $La_{0.5}Sr_{0.5}CoO_{3-d}$ [42], show quite high CTEs. Significantly, the CTE of $Ba_{0.5}Sr_{0.5}Co_{0.8}Fe_{0.2}O_{3-d}$ (BSCF) has almost the same value [33] as SBCO though Fe is not substituted in $SmBaCo_2O_{5+d}$. This observation indicates that SBCO:50 can minimize thermal mismatch between electrolyte and cathode material in SOFC operation.

Thermogravimetric analysis (TGA)–differential scanning calorimeter (DSC) results for SBCO are presented in Fig. 11 Two distinctive types of behaviour are observed in the vicinity of 300 and 530 °C. For the weight loss at 530 °C, when comparing the TGA-DSC results of PBCO ($PrBaCo_2O_{5+\delta}$) [44,45] and GBCO ($GdBaCo_2O_{5+\delta}$) [34], order–disorder phase transition in PBCO was observed [44,45] and the phase transition in GBCO was investigated at 500 °C [35].

Table 2
Specific coefficients of thermal expansion (CTEs) of SOFC materials between room temperature (RT) and 1000 °C [1,33,40–43].

Component	Materials	TEC ($\times 10^{-6} K^{-1}$) (RT-1000 °C)	Ref.
Electrolyte	8YSZ	10.5–11.0	[1,43]
	Doped ceria electrolyte	12–13.1	[43] In this experiment
	LSGM ($La_{0.9}Sr_{0.1}Ga_{0.8}Mg_{0.2}O_{3-d}$)	12.2	[42]
Cathode	SBCO	20.2	In this experiment
	SBCO:50	13.3	In this experiment
	$Sm_{0.5}Sr_{0.5}CoO_{3-d}$	22.3–22.8	[40,41]
	$La_{0.5}Sr_{0.5}CoO_{3-d}$	22.3	[42]
	$La_{0.6}Sr_{0.4}Co_{0.2}Fe_{0.8}O_{3-d}$	17.5	[42]
	$Ba_{0.5}Sr_{0.5}Co_{0.8}Fe_{0.2}O_{3-d}$	20.0	[33]

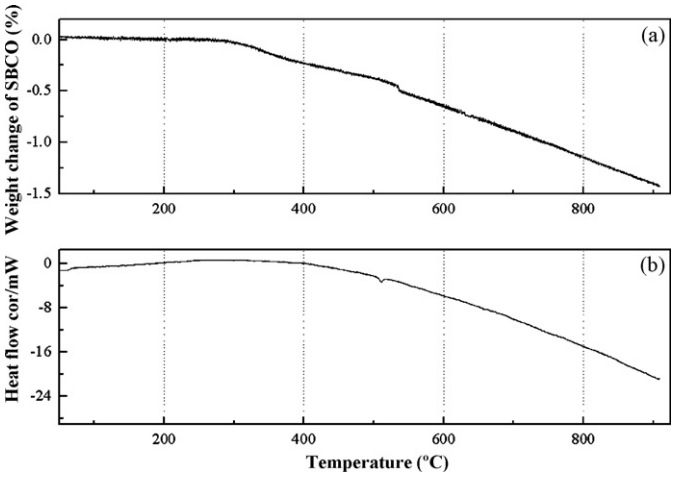

Fig. 11. TGA-DSC results of SBCO in air with increasing temperature. (a) and (b) TGA and DSC result of SBSCO.

The DSC data for SBCO reveal an enthothermic peak at 500 °C, as shown in Fig. 11(b). Thus the weight loss in the vicinity of 530 °C is related to a phase transition. Significantly, this abrupt weight loss occurs in the vicinity of 300 °C. As discussed before, the thermal expansion behaviour of SBCO shows slope changes at about 320 °C in Fig. 10(a). These TGA and thermal expansion findings confirm that the slope change at 300 °C is caused by the generation of oxygen vacancies.

4. Conclusions

The main objective of this research is to investigate the temperature-dependent electrical properties and thermal expansion properties of $SmBaCo_2O_{5+d}$ (SBCO).

SBCO shows semiconductor behaviour from room temperature to 250 °C, and metallic conductivity above 250 °C. The electrical conductivity of SBCO is always higher than 170 S cm^{-1} over the entire temperature range, and exhibits metallic and p-type conductor behaviour with respect to changes in oxygen partial pressure. The slope of $\log(p(O_2))$ is 1/6 and thereby indicates hole conduction behaviour in SBCO oxide at 700 °C. The ASR value of SBCO:50 on CGO91 is about 0.05 Ω cm^2 at 700 °C. The CTEs of SBCO are about 20.0×10^{-6} K^{-1} from 500 to 700 °C, i.e., much higher than those of CGO91 electrolyte. On the other hand, a composite cathode of SBCO:50 reduces their CTE values down to about 12.5×10^{-6} K^{-1} in the same region. These results are almost the same as those for CGO91 and the use of SBCO:50 can minimize thermal mismatch between the cathode and the electrolyte. Accordingly, SBCO:50 is a promising candidate cathode for IT-SOFC applications and has excellent conductivity, ASR and coefficients of CTE properties.

Acknowledgements

The authors are grateful for the support given by the Engineering and Physical Sciences Research Council (EPSRC) in United Kingdom and the Core Technologies for Fuel Cells (CTFC) of the Ministry of Knowledge Economy (MKE) of the Republic of Korea.

References

[1] N.Q. Minh, J. Am. Ceram. Soc. 76 (1993) 563–588.
[2] N.Q. Minh, T. Takahashi, Science and Technology of Ceramic Fuel Cell, Elsevier, New York, 1995, p. 1.
[3] T. Tsai, S.A. Barnett, Solid State Ionics 93 (1997) 207–217.
[4] J. Mizusaki, J. Tabuchi, T. Matsuura, S. Yamauchi, K. Fueki, J. Electrochem. Soc. 136 (1989) 2082–2088.
[5] Y. Teraoka, H.M. Zhang, K. Okamoto, N. Yamazoe, Mater. Res. Bull. 23 (1988) 51–58.
[6] S. Sekido, H. Tachibana, Y. Yamamura, T. Kamabara, Solid State Ionics 37 (1990) 253–259.
[7] H. Lv, B. Zhao, Y. Wu, G. Sun, G. Chen, K.-A. Hu, Mater. Res. Bull. 42 (2007) 1999–2012.
[8] W.Z. Zhou, C.T. Lin, W.Y. Ling, Adv. Mater. 5 (1993) 735–738.
[9] A. McKinlay, P. Connor, J.T.S. Irvine, W. Zhou, J. Phys. Chem. C 111 (2007) 19120–19125.
[10] F. Millange, V. Caignaert, B. Domengès, B. Raveau, E. Suard, Chem. Mater. 10 (1998) 1974–1983.
[11] T. Nakajima, H. Kageyama, Y. Ueda, J. Phys. Chem. Solids 63 (2002) 913–916.
[12] S. Trukhanov, I.O. Troyanchuk, M. Hervieu, H. Szymczak, K. Barner, Phys. Rev. B 66 (2002) 184424-1–184424-10.
[13] D. Akahoshi, M. Uchida, Y. Tomioka, T. Arima, Y. Matsui, Y. Tokura, Phys. Rev. Lett. 90 (2003) 177203-1–177203-4.
[14] J.-H. Kim, F. Prado, A. Manthirama, J. Electrochem. Soc. 155 (2008) B1023–B1028.
[15] J.-H. Kim, A. Manthiram, J. Electrochem. Soc. 155 (2008) B385–B390.
[16] C. Frontera, J.L. García-Muñoz, A. Llobet, L. Mañosa, M.A.G. Aranda, J. Solid State Chem. 171 (2003) 349–352.
[17] M. Respaud, C. Frontera, J.L. García-Muñoz, M.Á.G. Aranda, B. Raquet, J.M. Broto, H. Rakoto, M. Goiran, A. Llobet, J. Rodríguez-Carvajal, Phys. Rev. B 64 (2001) 214401-1–214401-7.
[18] C. Martin, A. Maignan, D. Pelloquin, N. Nguyen, B. Raveau, Appl. Phys. Lett. 71 (1997) 1421–1423.
[19] T. Albert, J. Skinner, J. Richard, F. Chater, Hernández-Ramírez, J.A. Kilner, J. Mater. Chem. 17 (2007) 3175–3181.
[20] A. Maignan, C. Martin, D. Pelloquin, N. Nguyen, B. Raveau, J. Solid State Chem. 142 (1999) 247–260.
[21] I.O. Troyanchuk, N.V. Kasper, D.D. Khalyavin, H. Szymczak, R. Szymczak, M. Baran, Phys. Rev. B 58 (1998) 2418–2421.
[22] P.S. Anderson, C.A. Kirk, J. Knudsen, I.M. Reaney, A.R. West, Solid State Sci. 7 (2005) 1149–1156.
[23] R.D. Sahnnon, Acta Crystallogr. A32 (1976) 751–767.
[24] T. Vogt, P.M. Woodward, P. Karen, B.A. Hunter, P. Henning, A.R. Moodenbaugh, Phys. Rev. Lett. 84 (2000) 2969–2972.
[25] E. Suard, F. Fauth, V. Caignaert, I. Mirebeau, G. Baldinozzi, Phys. Rev. B 61 (2000) R11871–R11874.
[26] C. Frontera, J.L. García-Muñoz, A. Llobet, M.A.G. Aranda, Phys. Rev. B 65 (2002) 180405-1–180405-4.
[27] F. Fauth, E. Suard, V. Caignaert, I. Mirebeau, Phys. Rev. B 66 (2002) 184421-1–184421-5.
[28] H. Kusuya, A. Machida, Y. Moritomo, K. Kato, E. Nishibori, M. Takata, M. Sakata, A. Nakamura, J. Phys. Soc. Jpn. 70 (2001) 3577–3580.
[29] H. Wu, Phys. Rev. B 64 (2001) 092413-1–092413-4.
[30] S.K. Kwon, J.H. Park, B.I. Min, Phys. Rev. B 62 (2000), R14 637–R14 640.
[31] G. Kim, S. Wang, A.J. Jacobson, L. Reimus, P. Brodersen, C.A. Mims, J. Mater. Chem. 17 (2007) 2500–2505.
[32] A. Tarancón, A. Morata, G. Dezanneau, S.J. Skinner, J.A. Kilner, S. Estrade, F. Hernández-Ramírez, F. Peiró, J.R. Morante, J. Power Sources 174 (2007) 255–263.

[33] W. Bo, L. Zhe, H. Xiqiang, M. Jipeng, S. Xueqing, X. Xianshuang, S. Wenhui, J. Eur. Ceram. Soc. 26 (2006) 2827–2832.
[34] L.-W. Tai, M.M. Nasrallah, H.U. Anderson, D.M. Sparlin, S.R. Sehlin, Solid State Ionics 76 (1995) 259–271.
[35] A. Tarancón, D. Marrero-López, J. Peña-Martínez, J.C. Ruiz-Morales, P. Núñez, Solid State Ionics 179 (2008) 611–618.
[36] K. Zhang, L. Ge, R. Ran, Z. Shao, S. Liu, Acta Mater. 56 (2008) 4876–4889.
[37] M. Ji-Woong, M. Yoshitake, S. Won-Seon, K. Kunihito, Mater. Sci. Eng. B85 (2001) 70–75.
[38] B.C.H. Steele, A. Heinzel, Nature 414 (2001) 345–352.
[39] H.Y. Tu, Y. Takeda, N. Imanishi, O. Yamamoto, Solid State Ionics 100 (1997) 283–288.
[40] Y. Shuo, H. Tianmin, H. Qiang, J. Alloys Compd. 450 (2008) 400–404.
[41] S.W. Baek, J.H. Kim, J. Bae, Solid State Ionics 179 (2008) 1570–1574.
[42] A. Aguadero, J.A. Alonso, M.T. Fernandez-Diaz, M.J. Escudero, L. Daza, J. Power Sources 169 (2007) 17–24.
[43] F. Tietz, Ionics 5 (1999) 129–139.
[44] S. Streule, A. Podlensyak, D. Sheptyakov, E. Pomjakushina, M. Stingaciu, K. Conder, M. Medarde, M.V. Patrakeev, I.A. Leonidov, V.L. Kozhevnikov, J. Mesot. Phys. Rev. B 73 (2006) 94203–94207.
[45] S. Streule, A. Podlensyak, E. Pomjakushina, K. Conder, D. Sheptyakov, M. Medarde, J. Mesot. Phys. B 378–380 (2006) 539–540.